Structural and Energetic Behavior of Mixed Samples in the Hexacosane (n-$C_{26}H_{54}$)/Octacosane (n-$C_{28}H_{58}$) System; Solid-Solid and Solid-Liquid Equilibria

by **Fazil Rajabalee**[1]), **Valérie Métivaud**[1]), **Denise Mondieig**[1])[2])*, and **Yvette Haget**[1])

Centre de Physique Moléculaire Optique et Hertzienne, UMR 5798 au CNRS – Université Bordeaux I, F-33405 Talence Cedex

Harry A. J. Oonk[1])

Petrology Group, Faculty of Earth Sciences and Chemical Thermodynamics Group, Faculty of Chemistry, Utrecht University, Padualaan 8, NL-3584 CH Utrecht

The combination of the experimental (microcalorimetric and X-ray diffraction) methods and thermodynamic analyses enabled us to determine the phase diagram of the system hexacosane (n-$C_{26}H_{54}$)/octacosane (n-$C_{28}H_{58}$). Isothermal X-ray measurements performed on mixed samples at 'low temperature' (T 308 K) revealed three crystalline forms: two monoclinic (M_{011} and M_{dci}) and one orthorhombic (O_p). Four of the five rotator phases were observed at 'high temperature': R_I, R_{II}, R_{IV}, and R_V. Fourteen solid-solid and two solid-liquid two-phase regions were observed, as well as one peritectic, one eutectoid, one metatectoid, and five peritectoid three-phase equilibria. The thermodynamic calculations of the phase-equilibrium relations, carried out with the polynomial functions described in a previous paper and new ones given here, showed full consistency with the experimental data, evidencing the reliability of these polynomial functions.

1. Introduction. – It is now commonly accepted that the structural behavior of (binary) mixed samples of normal alkanes C_nH_{2n+2} (hereafter denoted by C_n) is very complex [1–8]. Indeed, various 'ordered' forms (we will use quotation marks, because of the presence of substitutional disorder) are known to exist in the 'low-temperature' region (with respect to the high-temperature region where the rotator (R) and the liquid phases are observed). Recently, the ordered solid forms [4–8] in binary systems were identified structurally, and explanations have been given for their occurrence in the mixed samples [4][6]. One of the important findings is that mixing stabilizes forms that for unmixed alkanes become for the first time stable at higher values of n [4–8]. As an example, the rotator form R_I is encountered in the system C_{18}/C_{20} [4], of which the unmixed components C_{18} and C_{20} do not exhibit that form. One could say that conformational and rotational disorder are catalyzed by substitutional disorder. The aim of this work has been the determination of the structural and thermodynamic characteristics of the system {$(1-x)$ mol of $C_{26}+x$ mol of C_{28}} denoted by $C_{26}(1-x)/C_{28}(x)$.

---

[1]) All members of the REALM (Réseau Européen sur les ALliages Moléculaires)

[2]) Telephone: (33)556846988. Fax: (33)556846686. E-mail: dmondiei@frbdx11.cribx1.u-bordeaux.fr

2. Experimental. – Hexacosane (C_{26}) and octacosane (C_{28}) were purchased from *Fluka* and *Aldrich*, resp., with certified purity grades of 99% for C_{26} and 97% for C_{28}. Calorimetric measurements were carried out on a *Perkin-Elmer-DSC7* differential scanning calorimeter (DSC) operating in the sub-ambient mode. Transition temp. and enthalpies were obtained from at least four independent experiments on (4.0 ±)-mg samples with a scanning speed of $2\ K \cdot min^{-1}$. The shape-factor method [9][10] was used to determined the phase transition temperatures. The random part of the uncertainties was estimated using the *Student*'s method with 95% of threshold reliability.

Isothermal crystallographic measurements were performed using a *Siemens-D500* vertical powder diffractometer. A thin plate of glass was placed between the sample to be analyzed and the sample holder to avoid the diffraction reflections of copper and nickel which disturb the analyses of the diffractograms. The data were collected with a 0.05° 2θ step and 4 s interval time. Cu$K_{\alpha 1}$ radiation (λ 1.54056 Å) was used.

3. Results and Discussion. – 3.1. *Polymorphic Behavior of the Pure Components.* At room temperature, pure C_{26} gives rise to two different crystalline forms which are T_p and M_{011}, the stable and metastable ones, respectively [11]. The following two polymorphic sequences can be observed:

$$\mathbf{C_{26}}\begin{cases} M_{011} \xrightarrow{325.0\,K} R_{II} \xrightarrow{329.1\,K} \text{Liquid} \\ T_p \xrightarrow{<325.0\,K} R_{II} \xrightarrow{329.1\,K} \text{Liquid} \end{cases}$$

The form M_{011} is monoclinic with space group $P2_1/a$ ($Z=2$). The subscript '011' is used according to the notation introduced by *Sullivan* and *Weeks* [12]. The rotator form R_{II}, the most disordered among the five rotator forms, is hexagonal ($R\bar{3}m$ ($Z=3$)). The form T_p is triclinic with space group $P\bar{1}$ ($Z=1$). The subscript 'p' means 'pair', the French word for 'even'.

In the case of C_{28}, the stability relationships can be summarized as:

$$\mathbf{C_{28}}\begin{cases} M_{011} \xrightarrow{329.0\,K} R_{IV} \xrightarrow{333.0\,K} \text{Liquid} \\ O_p \xrightarrow{321.0\,K} M_{101} \xrightarrow{327.0\,K} R_{IV} \xrightarrow{333.0\,K} \text{Liquid} \end{cases}$$

M_{011} is monoclinic (see above), and the same holds true for M_{101} ($P2_1/a$, $Z=2$) and R_{IV}. The form O_p is orthorhombic ($Pca2_1$, $Z=4$).

In a melting and quenching (in liquid N_2) experiment, the forms M_{011} and O_p make their simultaneous appearance. A kinetic study [13] carried out at 298 K, just after melting and quenching, has shown that the amount of O_p decreases with time (exponentially during the first hour) while the amount of M_{011} increases. After several days, the O_p to M_{011} ratio is comparable to that obtained after melting and cooling to room temperature at a rate of $2\ K \cdot min^{-1}$. This study has allowed the author [13] to confirm that at 298 K, the M_{011} form is more stable than the O_p form.

For the phase-diagram determination, the following stable sequences are to be considered:

$$C_{26}: M_{011} \rightarrow R_{II} \rightarrow L$$
$$C_{28}: M_{011} \rightarrow R_{IV} \rightarrow L$$

3.2. *Mixed Samples – Experimental Results.* 3.2.1. *Preamble.* Twelve binary mixed samples were prepared as follows: the component substances were weighed in the

desired proportions and melted together. The melt was thoroughly stirred for homogenization and then quenched in liquid N_2. Isothermal diffraction studies at T 308 K were performed with all mixed samples, except for the sample with $x = 0.50$. The sample with $x = 0.30$ was studied by X-ray diffraction as a function of temperature. All twelve samples were analyzed by DSC in the temperature range 300 – 340 K.

3.2.2. *X-Ray Study at* T *308 K*. In addition to the M_{011} domains in the vicinity of the pure components, the X-ray analyses at 308 K enabled us to identify three intermediate single-phase fields. In the central compositional region, a single-phase field is found, pertaining to a monoclinic form denoted as M_{dcp}. The subscript 'dcp' is composed of 'dc' for 'défauts de conformation' (for conformational defects) and 'p' for 'pair' (the French word for 'even'). The other two intermediate single-phase fields are at the right- and left-hand sides of the M_{dcp} field and pertain to the form O_p (which is also found for pure C_{28}, be it under metastable conditions; see above). The experimental evidence is shown in *Fig. 1* for the relevant interval $37^\circ \leq 2\theta \leq 50^\circ$. The passage from M_{011} to O_p is marked by the disappearance of reflections at 2θ values of *ca.* 37.5, 39.2, 42.6, and 46.2° and the appearance of the reflections at *ca.* 42.1, 42.4, and 43.5°, and the passage from O_p to M_{dcp} by the disappearance of the lines at $2\theta \approx 42.1$ and 42.4° and the appearance of reflections at $2\theta \approx 42$, 42.5, 43, and 44.2°.

The M_{dcp} form has the same space group (Aa) and the same number of molecules per unit cell ($Z = 4$) as the M_{dci} form. The latter is found under stable conditions for pure C_{25} and pure C_{27} and also in a number of odd/odd and odd/even binary systems (see *Fig. 2*). The cell parameters of the O_p alloys for $x = 0.05$ and 0.85 and of the alloy M_{dcp} for $x = 0.61$ were determined at 308 K using the 'pattern-matching' option of the program FULLPROF [14] and are given in *Table 1*. Apart from cell refinement, this program yields also the calculated diffraction pattern and the differences between experimental and calculated intensities. In all three cases, the agreement is very good, and therefore, the cell parameters as well as the space groups can be considered as reliable. As an example, the experimental and calculated diffraction patterns of the mixed sample $C_{26}(0.39)/C_{28}(0.61)$ in the M_{dcp} form (Aa, $Z = 4$) is shown in *Fig. 3*.

Table 1. *Cell-Parameter Data at* T *308 K of the Mixed Samples $C_{26}(0.95)/C_{28}(0.05)$ and $C_{26}(0.15)/C_{28}(0.85)$ ($x =$* 0.05 and 0.85, resp.; O_p form) *and $C_{26}(0.39)/C_{28}(0.61)$* ($x = 0.61$; M_{dcp} form)

x of C_{28}	Forms	Group	Z	a [Å]	b [Å]	c [Å]	α[°]	β[°]	γ[°]
0.05	O_p	$Pca2_1$	4	7.52(2)	5.00(1)	70.05(4)	90	90	90
0.61	M_{dcp}	Aa	4	7.53(2)	5.01(1)	73.96(4)	90	91.0(6)	90
0.85	O_p	$Pca2_1$	4	7.51(2)	4.99(1)	75.22(3)	90	90	90

3.2.3. *Thermal Analysis*. The thermograms of all twelve mixed samples show two strong signals (see *Fig. 4*) that correspond to the transition from solid to rotator and to melting. In addition, thermograms for samples rich in C_{26} reveal a variation of the heat capacity due to the second-order transition from $R_V \dashrightarrow R_I$ and also a weak signal due to the first-order transition from R_I to R_{II}. As an example, the thermogram of the sample $C_{26}(0.70)/C_{28}(0.30)$ with $x = 0.30$ is given in *Fig. 5*. The $R_I \rightarrow R_{II}$ transition is difficult to observe, even in the enlargement (see *Fig. 5*,*b*).

3.2.4. *X-Ray Study of the Sample $C_{26}(0.70)/C_{28}(0.30)$*. X-Ray diffraction confirmed the observations made in *3.2.2*, as shown by *Figs. 6* and *7*. With increasing temperature,

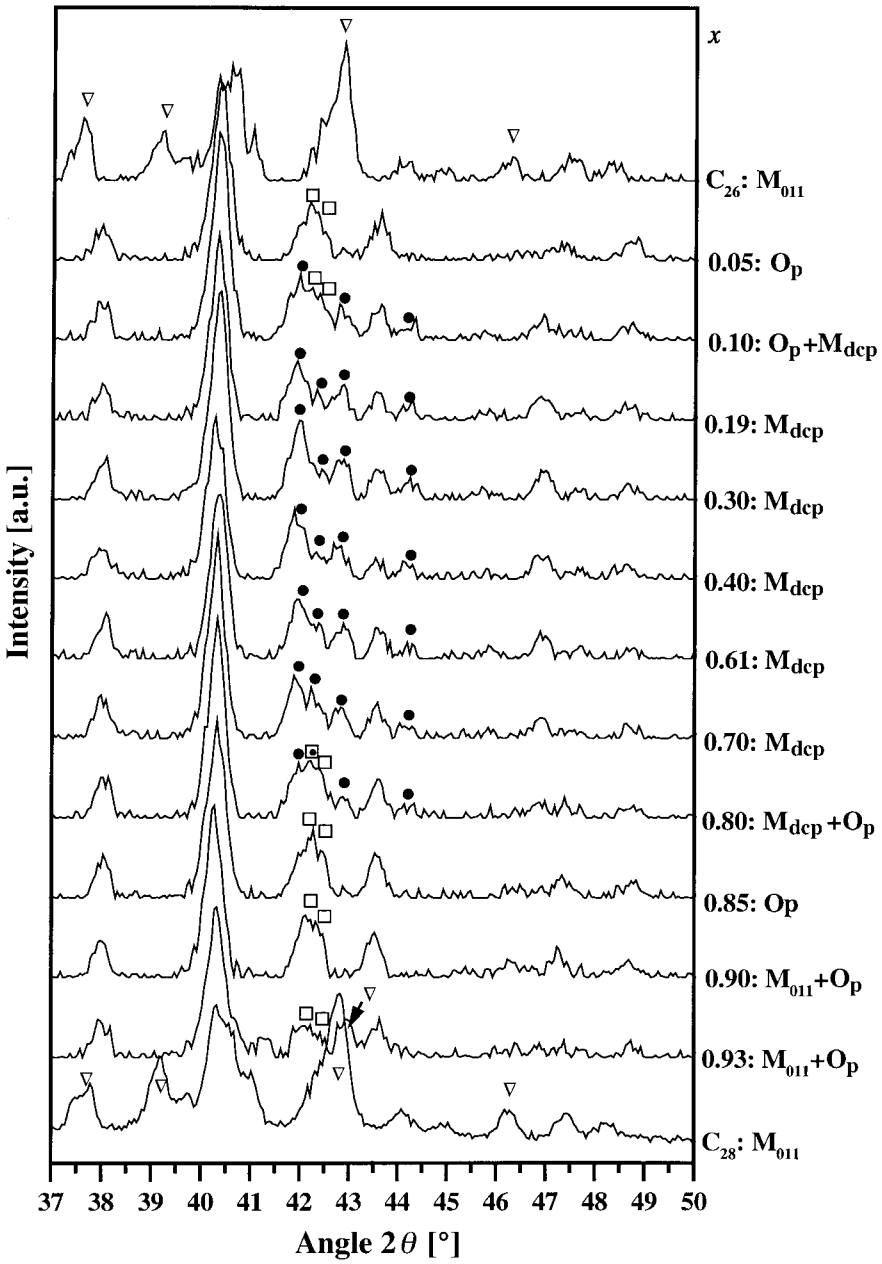

Fig. 1. *Isothermal X-ray diffraction patterns at* T *308 K as a function of mole fraction* x. The symbols ∇, □ and ● correspond to the M_{011}, O_p and M_{dcp} forms, respectively. They are used in the diffractogram to point out some reflections specific of one form which are not present in the other forms. The intensity is given in arbitrary units.

M_{dcp}: the letter 'M' stands for monoclinic and the subscript 'dcp' for 'défauts de conformation dans les alcanes pairs', the french words for conformational defects in the even alkanes.

O_p: the letter 'O' stands for orthorhombic and the subscript 'p' for 'pair', the French word for even. This form is orthorhombic and in pure alkanes, it is metastable and observed only in even alkanes.

M_{011}: the letter 'M' stands for monoclinic, and the subscript '011' denotes a shift of adjacent molecules in the (b,c) plane of a whole number of CH_2 units.

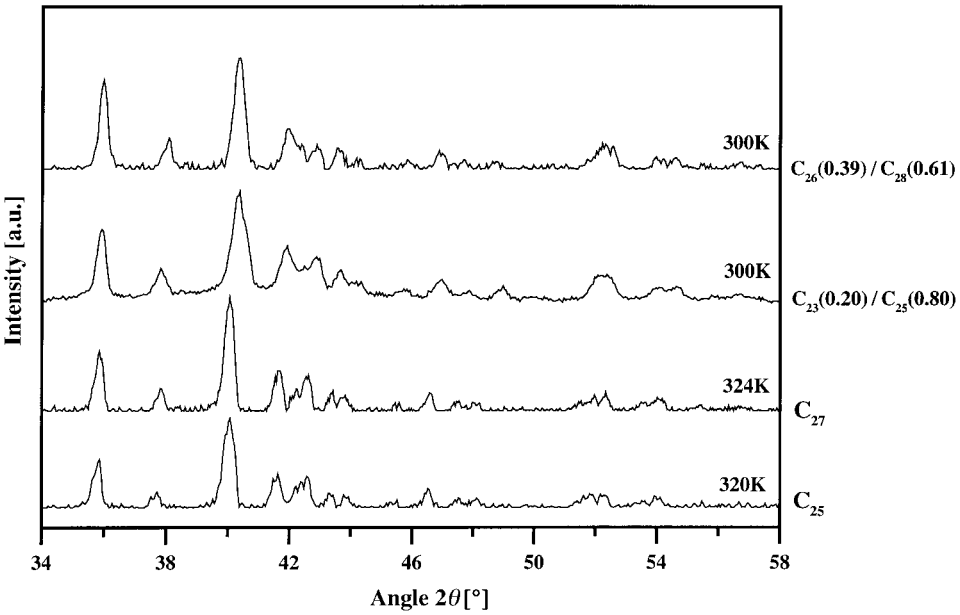

Fig. 2. *Comparison of the diffraction patterns of C_{25}, C_{27}, and the sample $C_{23}(0.20)/C_{25}(0.80)$ in the M_{dci} (Aa) form with that of the sample $C_{26}(0.39)/C_{28}(0.61)$ in the M_{dcp} (Aa) form*

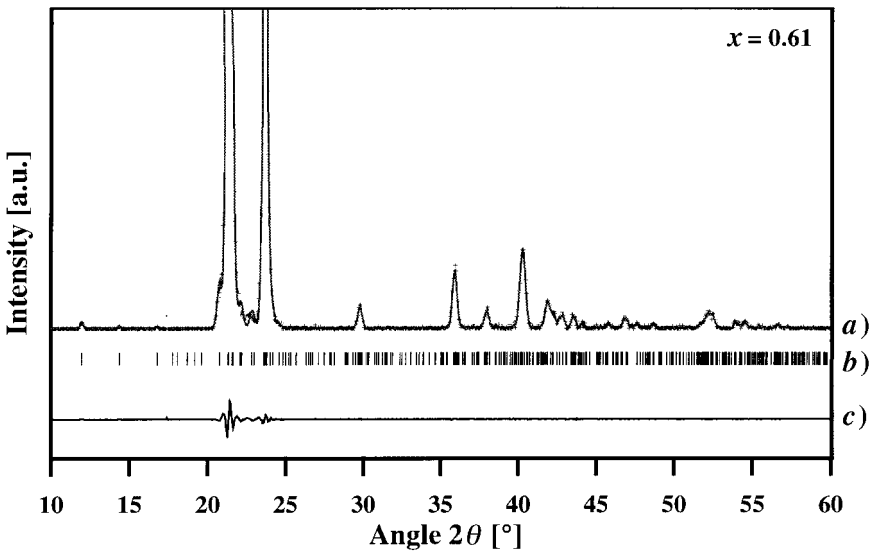

Fig. 3. a) *Experimental* (crosses) *and calculated* (line) *diffraction pattern of the mixed sample $C_{26}(0.39)/C_{28}(0.61)$ in the M_{dcp} (Aa) form*, b) *position of the calculated reflections, and* c) *difference between experimental and calculated intensities*

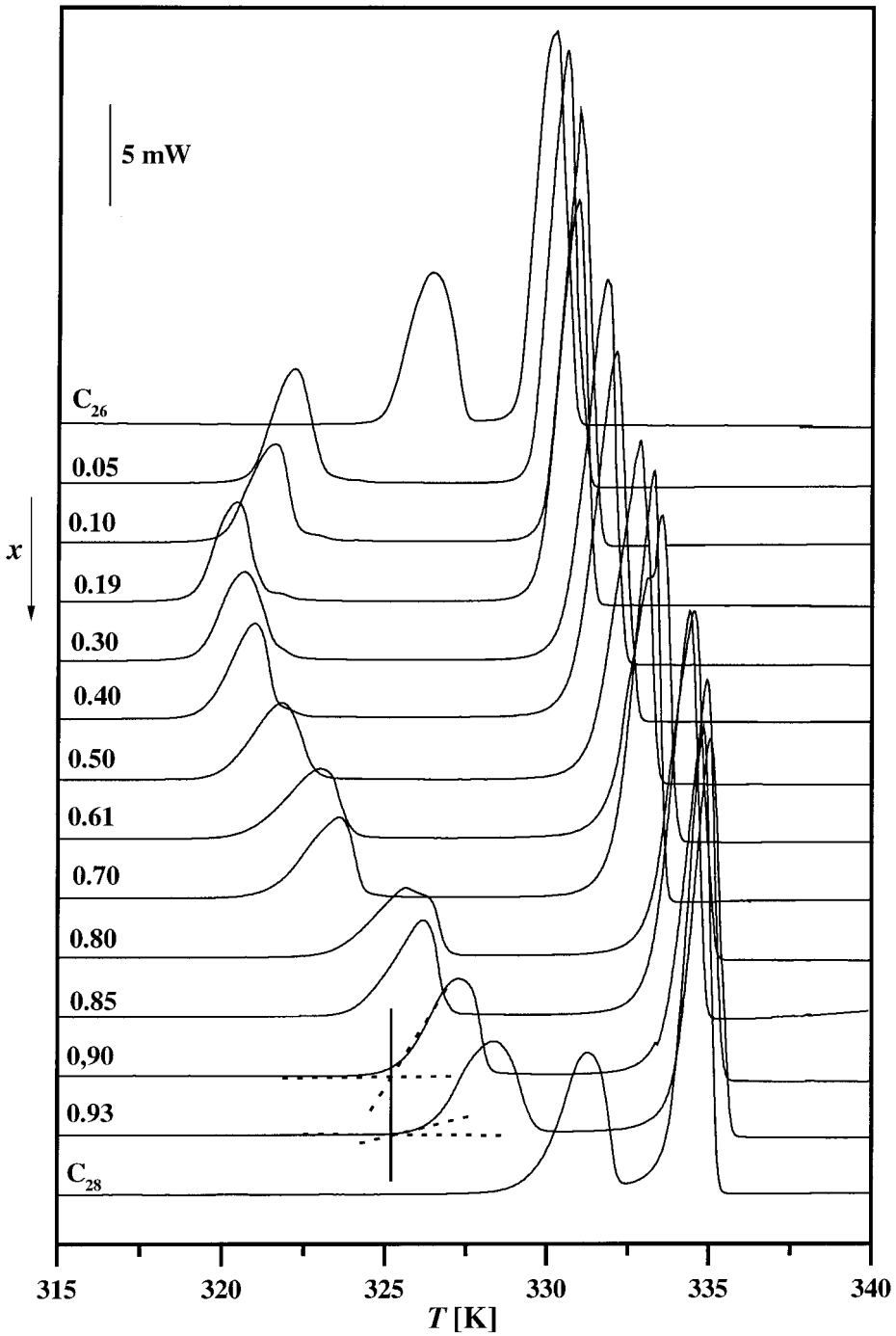

Fig. 4. *DSC Thermograms as a function of the mole fraction*

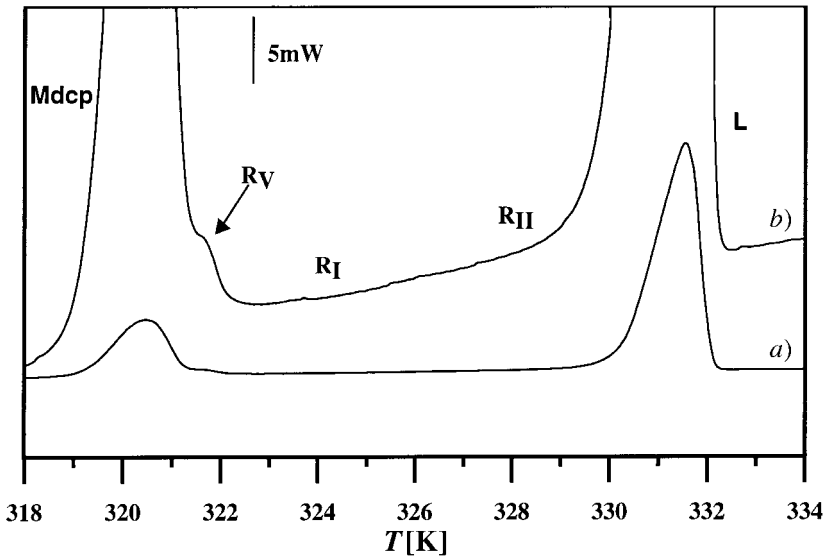

Fig. 5. *DSC Thermogram of the sample $C_{26}(0.70)/C_{28}(0.30)$:* a) *normal scale and* b) *amplified scale showing the second-order R_V ⇢ R_I transition* (the weakly energetic $R_I \rightarrow R_{II}$ is not perceptible)

the following sequence is observed $M_{dcp} \rightarrow R_V \dashrightarrow R_I \rightarrow R_{II}$. The existence of the rotator forms R_V and R_I, which, besides, are not observed for the pure components, follows from the presence of the two reflections (111) and (200) (see *Fig. 6*). In detail, the situation is as follows. At *T* 308 K, the sample is monoclinic M_{dcp}. The monoclinic R_V form appears at 320.5 K, reflected by the appearance of the diffraction line $(200)_{R_V}$ at $2\theta \approx 22.4°$; position does not change with temperature. The disappearance of the M_{dcp}

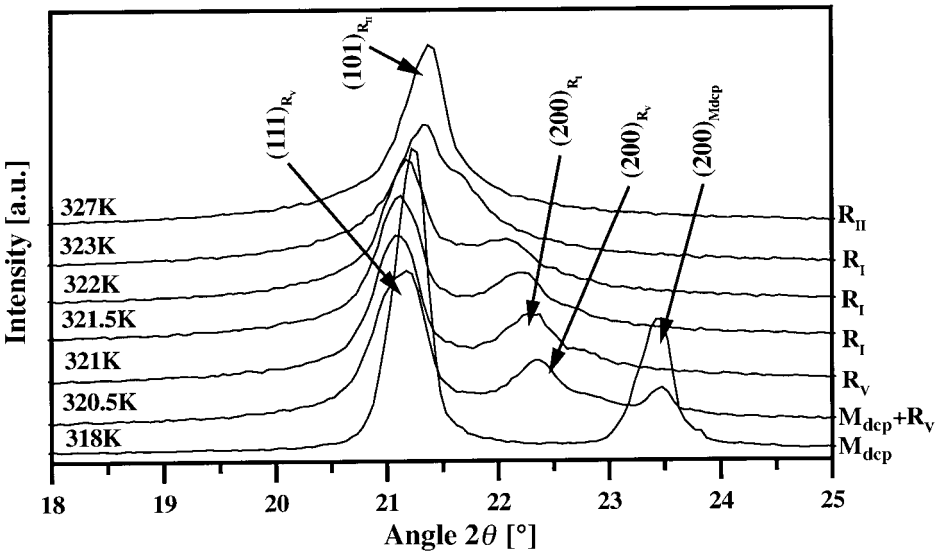

Fig. 6. *X-Ray-diffraction patterns of the sample $C_{26}(0.70)/C_{28}(0.30)$ at* T *318, 320.5, 321, 321.5, 322, 323, and 327 K*

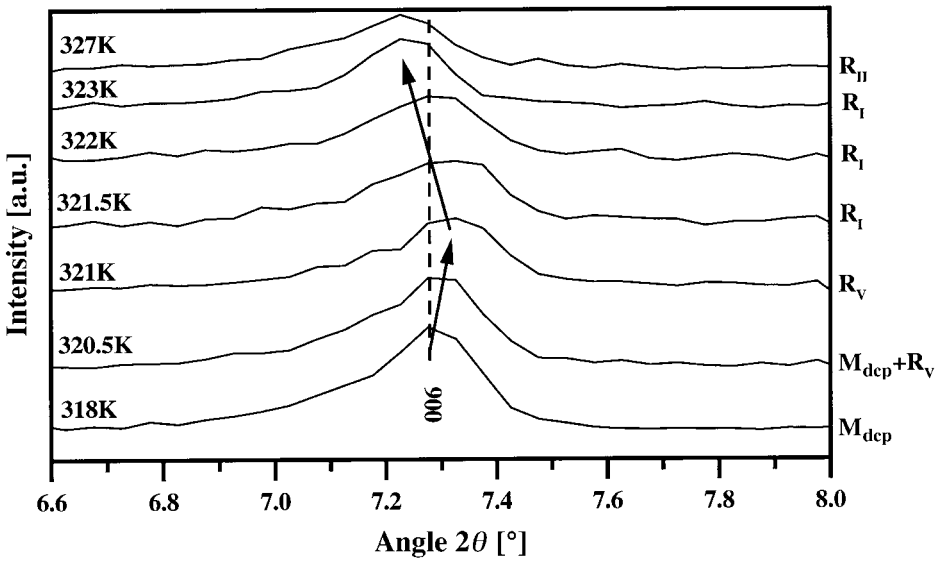

Fig. 7. *Evolution of the (006) reflection with temperature in the sample $C_{26}(0.70)/C_{28}(0.30)$*

form is observed when the $(200)_{M_{dcp}}$ line at $2\theta \approx 23.5^\circ$ vanishes, that is at T 321 K. The R_I form appears at T 321.5 K and is characterized by the shift towards lower angles of the $(200)_{R_I}$ and towards high angles for the $(111)_{R_I}$ reflection. In other words, with temperature rising, the cell parameter a increases while b decreases. Finally, the R_{II} form is characterized by a single peak, the $(101)_{R_{II}}$ in the range $18^\circ \leq 2\theta \leq 27^\circ$.

In the 2θ range examined above, it is quite difficult to distinguish between R_I and R_V. The study of the evolution of the $(00l)$ lines make it easier, since the R_V form is an inclined version of the R_I form [15][16]. *Fig. 7* shows the evolution of the (006) line with increasing temperature for the mixed sample $C_{26}(0.70)/C_{28}(0.30)$. We can observe a weak shift towards higher angles of the line from T 318 K to T 321 K, synonymous of the presence of the R_V phase. Indeed, the β angle of the monoclinic M_{dcp} form being very close to 90°, the transition from M_{dcp} to R_V induces a decrease of the interlayer spacing. From 321 K on, the reflection (006) shifts towards lower angles due to the thermal expansion.

3.3. *The Experimental Phase Diagram and Energetic Data.* From the combined structural and thermal analytical data on pure components and mixed samples, we constructed the phase diagram shown in *Fig. 8*. It has nine single-phase fields and 16 two-phase fields. The single-phase fields are $[M_{011,C_{26}}]$, $[O_{p,C_{26}}]$, $[M_{dcp}]$, $[O_{p,C_{28}}]$, $[M_{011,C_{28}}]$, $[R_{IV}]$, $[R_{II}]$, $[R_I]$, and [L] and the two-phase fields are $[M_{011,C_{26}} + Op_{,C_{26}}]$, $[O_{p,C_{26}} + M_{dcp}]$, $[M_{dcp} + O_{p,C_{28}}]$, $[O_{p,C_{28}} + M_{011,C_{28}}]$, $[R_{IV} + M_{011,C_{28}}]$, $[R + M_{011,C_{28}}]$, $[O_{p,C_{28}} + R]$, $[M_{dcp} + R]$, $[O_{p,C_{26}} + R]$, $[M_{011,C_{26}} + R_{II}]$, $[R_I + R_{II}]$, $[R_{II} + R_{IV}]$, $[R_I + R_{IV}]$, $[R_{II} + L]$, $[R_{IV} + L]$, and $[M_{011,C_{26}} + R]$. There are eight three-phase equilibria of which one is peritectic, five are peritectoid, and two are metatectoid. Details on the data points – shown in the experimental phase diagram (*Fig. 8*) and obtained by thermal analysis – are given in *Tables 2* and *3*, along with the measured heat effects.

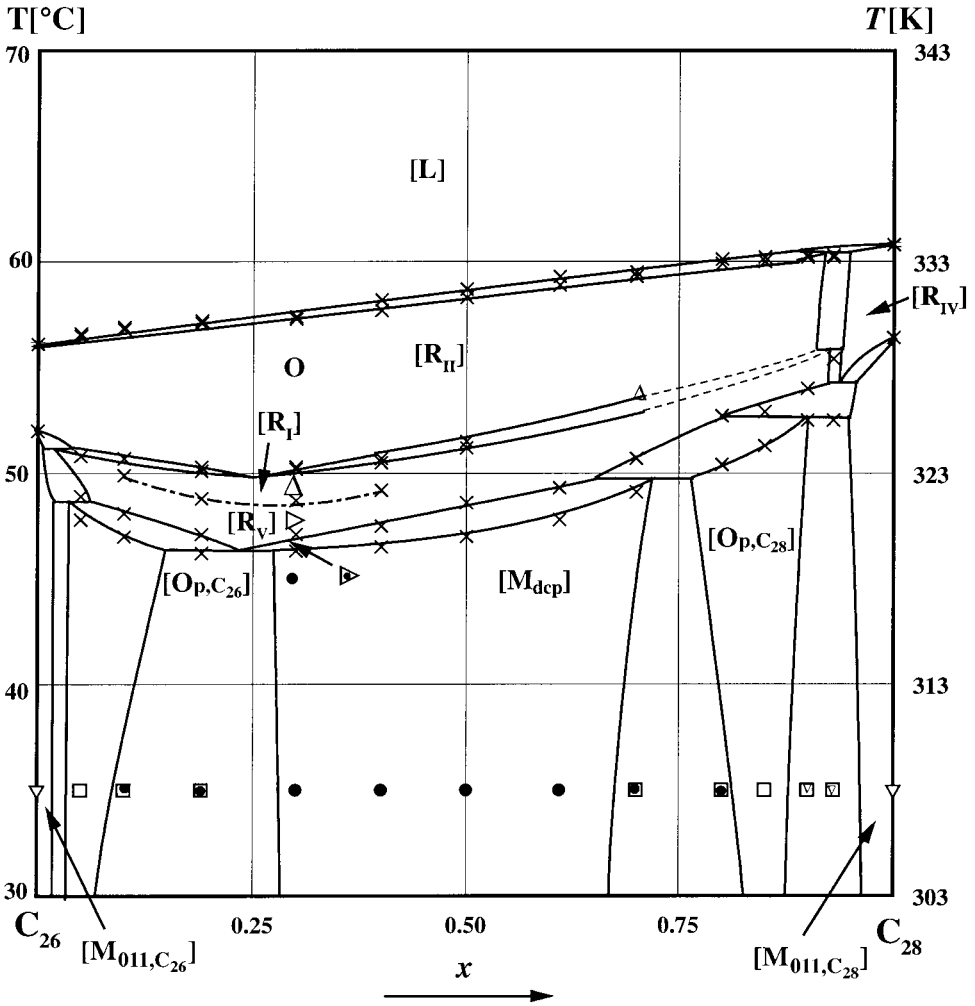

Fig. 8. *Phase diagram of C_{26}/C_{28} as determined by DSC and X-ray diffraction.* × : DSC Data. ∇, □, •, △, and ○: X-Ray data for $M_{011,\,Op}$, M_{dcp}, R_V, R_I, and R_{II}, resp.

The ensemble of phase diagram and energetic data gives rise to a number of observations. To start with, the heat effect of the transition $R_I \rightarrow R_{II}$ is very small (*ca.* 0.3 kJ · mol^{-1}) and is not included in *Table 2*. As regards the heat effect of melting, in spite of the experimental uncertainties, one can observe that the heat of melting as a function of composition has a somewhat convex nature. For the equimolar composition, it would correspond to a value that is *ca.* 1 kJ · mol^{-1} lower than the arithmetic mean of the heats of melting of the two components (expressed in other terms: the excess enthalpy of melting of the equimolar mixture, ΔH^E ($x = 0.5$), is *ca.* -1 kJ · mol^{-1}). In the case of the heat effects given in *Table 3*, pertaining to the transition from 'ordered' solid to rotator, the effect at equimolar composition is *ca.* 45% lower than the mean. The great difference is due to the difference in form, *i.e.*, M_{dcp} *vs.* M_{011}, and, in

Table 2. *Thermoenergetic Data for the Rotator → Rotator Transitions (*$R_V \dashrightarrow R_I$ and $R_I \rightarrow R_{II}$*) and for Melting*

x of C_{28}	Transition $R_V \dashrightarrow R_I$	Transition $R_I \rightarrow R_{II}$		Melting		
		T_{solvi} [K]	T_{solvs} [K]	T_{sol} [K]	T_{liq} [K]	ΔH_f [kJ·mol^{-1}]
C_{26}				329.1 ± 0.1		60.1 ± 1.5
0.05	–[a])	323.9 ± 0.2	324.1 ± 0.1	329.3 ± 0.2	329.4 ± 0.2	59.9 ± 1.2
0.10	322.9 ± 0.2	323.7 ± 0.3	323.7 ± 0.2	329.5 ± 0.3	329.6 ± 0.1	59.8 ± 1.4
0.19	321.8 ± 0.3	323.1 ± 0.2	323.3 ± 0.1	330.1 ± 0.4	330.2 ± 0.2	60.0 ± 1.2
0.30	321.7 ± 0.3	323.2 ± 0.4	323.3 ± 0.2	330.3 ± 0.5	330.9 ± 0.4	60.4 ± 1.2
0.40	322.2 ± 0.4	323.5 ± 0.4	323.7 ± 0.3	330.7 ± 0.4	331.2 ± 0.3	60.4 ± 1.3
0.50		324.2 ± 0.3	324.3 ± 0.3	331.3 ± 0.2	331.7 ± 0.1	60.6 ± 1.6
0.61				331.9 ± 0.2	332.3 ± 0.2	60.7 ± 1.2
0.70				332.3 ± 0.3	332.5 ± 0.1	61.4 ± 1.1
0.80				332.6 ± 0.4	332.9 ± 0.3	61.4 ± 0.9
0.85				332.8 ± 0.4	333.1 ± 0.1	61.8 ± 1.4
0.90				333.2 ± 0.3	333.2 ± 0.2	62.1 ± 0.9
0.93				333.2 ± 0.2	333.3 ± 0.2	62.3 ± 1.3
C_{28}				333.4 ± 0.1		63.0 ± 1.5

[a]) Observable but not easy to characterize.

Table 3. *Thermoenergetic Data for the Transitions from the 'Ordered' to Rotator Form*

x of C_{28}	(M_{011}, O_p, or M_{dcp}) → Rotator R phase transitions					
	Phase(s) concerned	T_{solvi} [K]	T_E [K]	T_P [K]	T_{solvs} [K]	ΔH_{tr} [k·mol]
C_{26}	M_{011}	325.0 ± 0.1				32.6 ± 1.1
0.05	O_p	320.8 ± 0.3			321.9 ± 0.3	21.3 ± 0.9
0.10	O_p	320.0 ± 0.2			321.1 ± 0.1	20.8 ± 0.5
0.19	$O_p + M_{dcp}$		319.2 ± 0.1		320.1 ± 0.2	
0.30	M_{dcp}	319.3 ± 0.4			320.1 ± 0.2	18.4 ± 0.4
0.40	M_{dcp}	319.5 ± 0.4			320.5 ± 0.3	18.6 ± 0.3
0.50	M_{dcp}	320.0 ± 0.2			321.6 ± 0.1	18.6 ± 0.5
0.61	M_{dcp}	320.8 ± 0.3			322.3 ± 0.3	19.1 ± 0.5
0.70	M_{dcp}	322.1 ± 0.4			323.7 ± 0.2	19.3 ± 0.4
0.80	O_p	323.4 ± 0.3			325.7 ± 0.3	19.5 ± 0.6
0.85	O_p	324.3 ± 0.2		–[a])	325.9 ± 0.1	
0.90	$O_p + M_{011}$			325.5 ± 0.2	327.0 ± 0.2	
0.93	$O_p + M_{011}$			325.5 ± 0.1		
C_{28}	M_{011}	329.4 ± 0.1				35.2 ± 1.2

[a]) Temperature data difficult to obtain.

particular, to the larger positive excess enthalpies (heats of mixing) in the 'ordered' solid forms.

3.4. *Thermodynamic Calculations.* The equilibria $[R_{II} + L]$, $[R_I + R_{II}]$, $[O_p + R]$, and $[M_{dcp} + R]$, which in the phase diagram give rise to rather wide domains in composition, were subjected to a thermodynamic analysis, one after the other in the order given. The methodology, which has been detailed in our paper on the system C_{23}/C_{25} [8], can be summarized as follows: In an iterative procedure of phase-diagram calculations, by means of the procedure LIQFIT [17], the calculated equilibrium curve at the high-temperature side of the phase diagram is made to pass through the

experimental data. Apart from the experimental phase-diagram data, meant in the foregoing phrase, the input of LIQFIT consists of the transition temperatures and transition entropies of the pure components. The adjustable parameters of the iterative procedure are $\Delta_\alpha^\beta G_1$ and $\Delta_\alpha^\beta G_2$, the system-dependent constants of the expression for the excess *Gibbs*-energy difference of the forms α and β (*e.g.*, $\alpha = R_I$ and $\beta =$ liquid):

$$\Delta_\alpha^\beta G^E(T,x) = \Delta_\alpha^\beta G^E(x) = x(1-x)\{\Delta_\alpha^\beta G_1 + (1-2x)\Delta_\alpha^\beta G_2\}$$

After having carried out the computations, the difference properties $\Delta_\alpha^\beta G_1$ and $\Delta_\alpha^\beta G_2$ are split up in G_1^α and G_2^α and G_1^β and G_2^β, which is possible after having taken $G_1^{liq} = 0$ and $G_2^{liq} = 0$.

In *Table 4*, the pure-component input data are summarized; they need the following additional explanation. The (metastable) $R_{II} \rightarrow L$ transition temperature of C_{28}, *i.e.*, the metastable melting point of the R_{II} form, was obtained by extrapolation (see *Fig. 9*) using the formula

$$T_m\ (R_{II} \rightarrow L)\ [K] = 152.16 + 11.168\ \cdot\ n - 0.1679\ \cdot\ n^2$$

Likewise, the (metastable) transition points for $R_I \rightarrow R_{II}$, for both C_{26} and C_{28}, were calculated as

$$T_{tr}(R_I \rightarrow R_{II})\ [K] = 324.31 - 2.497\ \cdot\ n + 0.0964 \cdot n^2$$

The entropy changes given in *Table 4* for the transition $R_I \rightarrow R_{II}$ are the result of taking for the enthalpy effect the same small value of $340\ J \cdot mol^{-1}$ for C_{26} and C_{28}.

Table 4. *Input Data for LIQFIT Computations, Consisting of Entropies of Transition and Temperatures of Transition for C_{26} and C_{28}*

α	β	$\Delta_\alpha^\beta S^*_{C_{26}}$ [$J \cdot K^{-1} \cdot mol^{-1}$]	$T^{\alpha\rightarrow\beta}_{C_{26}}$[K]	$\Delta_\alpha^\beta S^*_{C_{28}}$ [$J \cdot K^{-1} \cdot mol^{-1}$]	$T^{\alpha\rightarrow\beta}_{C_{28}}$[K]
R_{II}	L	182.6	329.1	194.1	333.3
R_I	R_{II}	1.05	324.6	1.03	330.0
O_p	R	76.5	322.2	87.5	328.0
M_{dcp}	R	77.2	319.4	87.9	326.5

As for the heat effects of the transition from 'ordered' solid to the rotator form, we have [6] the following formula:

$$\Delta H_{tr}\ [kJ \cdot mol^{-1}] = 5.44 - 0.462 \cdot n + 0.0462\ \cdot\ n^2$$

independent of the nature of the 'ordered' and rotator forms involved.

For the temperatures of transition, we proposed [6] the following formulae:

$$T_{tr}(O_p \rightarrow R)\ [K] = 107.63 + 13.220 \cdot n - 0.1911 \cdot n^2$$

$$T_{tr}(M_{dcp} \rightarrow R)\ [K] = 76.66 + 14.900 \cdot n - 0.2143 \cdot n^2$$

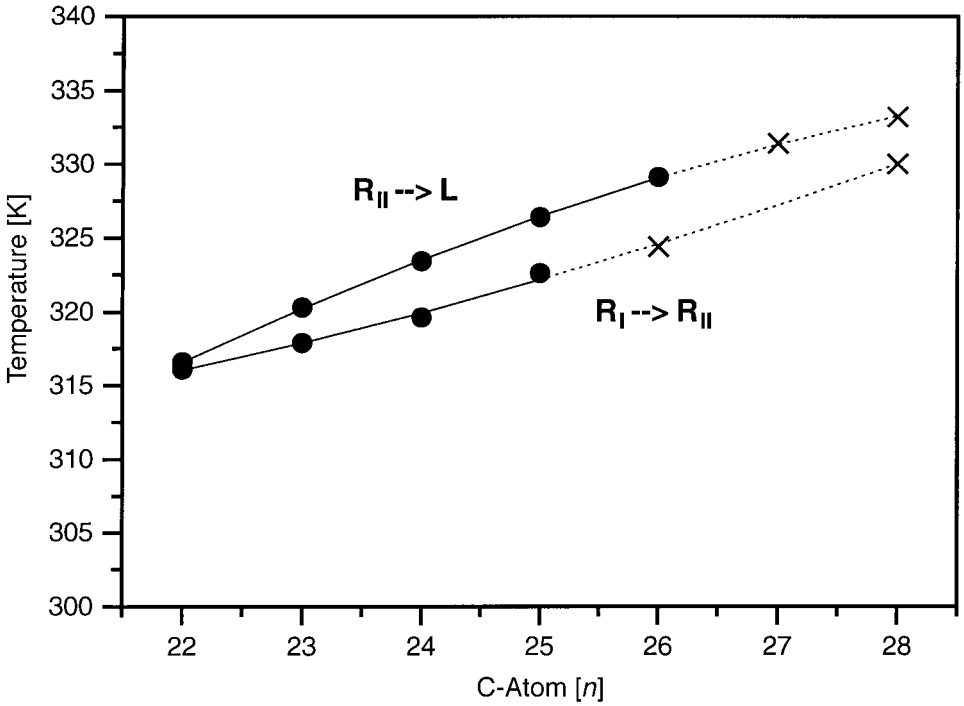

Fig. 9. *Variation of the $R_I \rightarrow R_{II}$ and $R_{II} \rightarrow L$ temperature phase* (stable) *transitions with chain length* n *for C_{22} to C_{26} (•) and extrapolation to C_{27} and C_{28} (×)*

The output of the LIQFIT computation consists of the phase diagrams shown in *Fig. 10*, and the constants G_1 and G_2 of the expressions for the excess *Gibbs* energies are given in *Table 5*.

The overall agreement between the experimental data and the calculated phase diagram is quite satisfactory; it means that the ensemble of estimated properties and experimentally known properties is internally consistent. Notwithstanding that, a few words may be said about the $[M_{dcp} + R_I]$ loop (see *Fig. 10,a*). The calculated loop is narrower than the experimental data would suggest, which, besides, is not an uncommon observation for the kind of systems studied. LIQFIT Computations usually are carried out such that the agreement is obtained with the data at the high-temperature side rather than with the data at the low-temperature side (thermodynamic equilibrium is more easily realized at the high-temperature side of the transition than at the low-temperature side). The combination of the calculated $[M_{dcp} + R_I]$ and $[O_p + R_I]$ loops corresponds to an eutectoid type of three-phase equilibrium at T 319.2 K and a peritectoid type at T 322.5 K; in the experimental diagram (*Fig. 8*), these temperatures are T 320.0 K and 322.9 K, respectively.

4. Conclusion. – The X-ray and thermal analytical study of the system C_{26}/C_{28} revealed a complex phase diagram which can be summarized as follows. Apart from the liquid single-phase field, the widest domain is that of the form R_{II}, which is the most

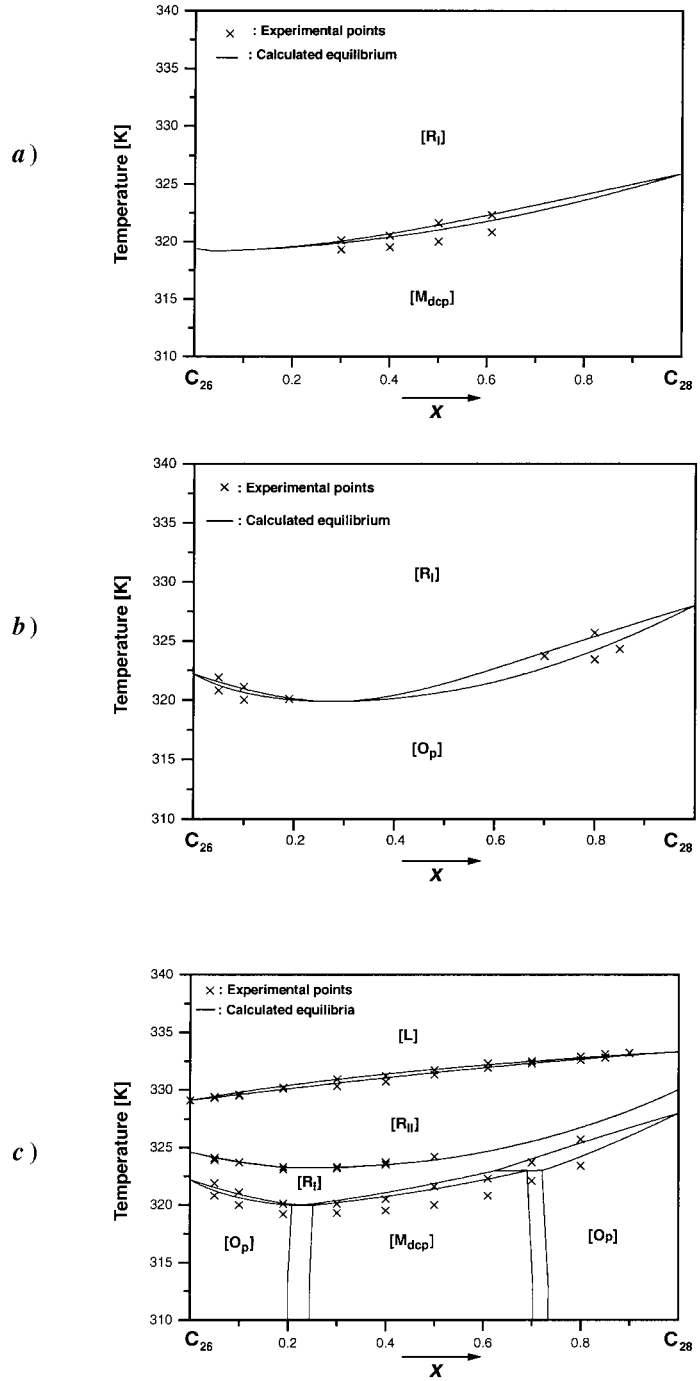

Fig. 10. *Calculated phase diagram* (for the equilibria treated) *along with the experimental points:* a) *[M_{dcp} + R] loop*, b) *[O_p + R] loop*, c) *complete diagram*

Table 5. *Computed Values of the Coefficients* G_1 *and* G_2 *of the Excess* Gibbs *Energy functions*

	R_{II}	R_I	O_p	M_{dcp}
$G_1[J \cdot mol^{-1}]$	– 280	– 266	1150	250
$G_2[J \cdot mol^{-1}]$			470	100

disordered among the five rotator forms. R_{II} is observed under stable conditions for C_{26} but not for C_{28}; for the latter, the stable rotator form is R_{IV}. The R_{IV} single-phase field extends over just 10% of the mole-fraction scale. In addition, the rotator forms R_I and R_V, not stable for the components of the system, make their appearance. At the low-temperature side, M_{011} is the stable form of both C_{26} and C_{28}; in the direction of the equimolar composition, it makes room first for the orthorhombic form O_p and then for the monoclinic form M_{dcp}. Single-phase fields of O_p and M_{dcp} are observed also in other even/even systems like C_{18}/C_{20} [4] and C_{22}/C_{24} [4].

For reasons outlined in our work on the system C_{23}/C_{25} [8], we used temperature-independent excess *Gibbs* energies to support our experimental observations by thermodynamic phase-diagram computations. The agreement between the outcome of these calculations and the experimental data is very satisfactory. The real physical nature of the excess *Gibbs* energy will be the subject of a report of more global nature, *i.e.*, concerning the whole group of mixed crystals of the 'ordered' type.

REFERENCES

[1] H. Luth, S. C. Nyburg, P. M. Robinson, H. E. Scott, *Mol. Cryst. Liq. Cryst.* **1974**, *27*, 337.
[2] A. R. Gerson, S. C. Nyburg, *Acta Crystallogr., Sect. B* **1994**, *50*, 252.
[3] M. Dirand, Z. Achour, B. Jouti, A. Sabour, J. C. Gachon, *Mol. Cryst. Liq. Cryst.* **1996**, *275*, 293.
[4] F. Rajabalee, European Label Thesis, University Bordeaux I, France, 1998.
[5] V. Métivaud, F. Rajabalee, D. Mondieig, Y. Haget, M. A. Cuevas-Diarte, *Chem. Mater.* **1999**, *11*, 117.
[6] F. Rajabalee, V. Métivaud, D. Mondieig, Y. Haget, M. A. Cuevas-Diarte, *J. Mat. Res.*, in press.
[7] V. Métivaud, F. Rajabalee, M. A. Cuevas-Diarte, T. Calvet, D. Mondieig, Y. Haget, *An. Quim.*, in press.
[8] F. Rajabalee, V. Métivaud, H. A. J. Oonk, D. Mondieig, Y. Haget, submitted to *Chem. Mater.*
[9] R. Courchinoux, N. B. Chanh, Y. Haget, E. Tauler, M. A. Cuevas-Diarte, *Thermochim. Acta* **1988**, *128*, 45.
[10] R. Courchinoux, N. B. Chanh, Y. Haget, T. Calvet, E. Estop, M. A. Cuevas-Diarte, *J. Chim. Phys.* **1989**, *86*, 561.
[11] L. Robles, D. Mondieig, Y. Haget, M. A. Cuevas-Diarte, *J. Chim. Phys.* **1998**, *95*, 92.
[12] P. K. Sullivan, J. J. Weeks, *J. Res. NBS A* **1970**, *74*, 203.
[13] B. Poirier, Thesis, University Bordeaux I, France, 1996.
[14] J. Rodriguez-Carvajal, 'FULLPROF, a Program for *Rietveld* Refinement and Pattern Matching Analyses', Abstracts of the Satellite Meeting on Powder Diffraction on the XVth Congress of the International Union of Crystallography, Toulouse, 1990, p. 117.
[15] E. B. Sirota, H. E. King Jr., D. M. Singer, H. H. Shao, *J. Chem. Phys.* **1993**, *98*, 5809.
[16] E. B. Sirota, H. E. King Jr., H. H. Shao, D. M. Singer, *J. Phys. Chem.* **1995**, *99*, 798.
[17] M. H. G. Jacobs, H. A. J. Oonk, 'LIQFIT, a Computer Program for the Thermodynamic Assessment of Vaporus, Liquidus, Solidus Curves in TX Phase Diagrams (Version 1.2)', Chemical Thermodynamics Group, Utrecht University, 1989.

Received June 15, 1999